Tuning the Fabrication of Nanostructures by Low-Energy Highly Charged Ions

Ayman S. El-Said,[1,*] Richard A. Wilhelm,[2,3] Rene Heller,[2] Michael Sorokin,[4] Stefan Facsko,[2] and Friedrich Aumayr[3,†]
[1]Physics Department, King Fahd University of Petroleum and Minerals, Dhahran 31261, Saudi Arabia
[2]Institute of Ion Beam Physics and Materials Research, Helmholtz-Zentrum Dresden-Rossendorf (HZDR), 01328 Dresden, Germany
[3]Institute of Applied Physics, Vienna University of Technology, 1040 Vienna, Austria
[4]National Research Centre "Kurchatov Institute," Kurchatov Square 1, 123182 Moscow, Russia
(Received 9 June 2016; published 13 September 2016)

Slow highly charged ions have been utilized recently for the creation of monotype surface nanostructures (craters, calderas, or hillocks) in different materials. In the present study, we report on the ability of slow highly charged xenon ions ($^{129}Xe^{Q+}$) to form three different types of nanostructures on the LiF(100) surface. By increasing the charge state from $Q = 15$ to $Q = 36$, the shape of the impact induced nanostructures changes from craters to hillocks crossing an intermediate stage of caldera structures. A dimensional analysis of the nanostructures reveals an increase of the height up to 1.5 nm as a function of the potential energy of the incident ions. Based on the evolution of both the geometry and size of the created nanostructures, defect-mediated desorption and the development of a thermal spike are utilized as creation mechanisms of the nanostructures at low and high charge states, respectively.

DOI: 10.1103/PhysRevLett.117.126101

In recent years, ion beam technology has demonstrated its uniqueness and effectiveness in the synthesis and precise control of nanostructures in various materials [1–3]. Both swift heavy ions (SHIs) and slow highly charged ions (HCIs) are especially efficient in creating nanostructures via single ion impacts; i.e., each ion creates one nanostructure. However, HCIs have a significant advantage over SHIs in that the nanostructures are created only at the surface without modifying the bulk of the material [4]. Depending on their structure and properties the materials respond differently to the energy deposition by HCIs, resulting in different types of nanostructures. In the case of CaF_2, BaF_2, Muscovite mica, SiO_2, $SrTiO_3$, Al_2O_3, and HOPG, nanohillocks were observed [5–12], whereas craters (pits) were created in Si, PMMA, KBr, KCl, and carbon nanomembranes [13–15]. Furthermore, caldera structures were formed in $TiO_2(110)$ [16]. In addition, pyramidal pits were created in the surfaces of CaF_2 and BaF_2 by means of selective chemical etching [5,6]. For each material investigated so far only one type of nanostructures induced by single HCI impacts has been observed [4].

In this Letter, we report on the creation of three different types of nanostructures in one material, namely, crystalline lithium fluroride (LiF), after irradiation with HCIs of different charge states. LiF has a wide band gap of 14.6 eV and highly stable radiation-induced color centers at RT. These characteristics make LiF a prospective material for many applications such as laser sources, wave guides, and dosimetry [17–19]. Moreover, LiF films were grown epitaxially on Si(100), opening the possibility of using LiF as an insulating material in silicon based devices [20]. In view of these applications, the nanostructuring of LiF by ions has technological relevance.

LiF belongs to the class of ionic flouride materials (e.g., LaF_2, MgF_2, CaF_2, and BaF_2). They were intensively studied after irradiation with SHIs [21–24]. The deposition of the large kinetic energy of SHIs causes strong electronic excitation and ionization in a localized zone. As a result, different kinds of modifications were induced in both the surface and bulk of LiF and the other ionic crystals. Among all the investigated fluorides, LiF exhibits the highest efficiency for the creation of color centers and for volume swelling, with a strong dependence on ion fluence and electronic energy loss (dE/dx) [21,25,26].

The interaction of SHIs with the fluoride ionic single crystals is accompanied by the creation of surface hillocks provided that a threshold in (dE/dx) of ~5.0 keV/nm is exceeded. The size of these hillocks was observed to increase as a function of (dE/dx) [27–29]. Several recent experiments using HCIs showed the formation of similar nanostructures. This similarity suggests a common mechanism regarding the transfer of the electronic excitations to the lattice of the irradiated material [4]. The deposition of the potential energy E_p of the HCIs, i.e., the sum of the binding energy of all missing electrons, plays the same role as dE/dx of the SHIs for the creation of surface nanostructures.

The samples for the present study are thin platelets of 1.0 cm^2 area and ~0.5 mm thickness, mechanically cleaved in ambient atmosphere along the (100) plane from a $1.0 \times 1.0 \times 5$ cm^3 LiF single-crystal block (Korth Kristalle, Germany). The freshly cleaved samples were irradiated at normal incidence with highly charged $^{129}Xe^{Q+}$ ions of different charge states in the range of $Q = 15$ to $Q = 36$, corresponding to a wide range of potential energies between $E_p = 2.2$ keV and $E_p = 27.8$ keV. The

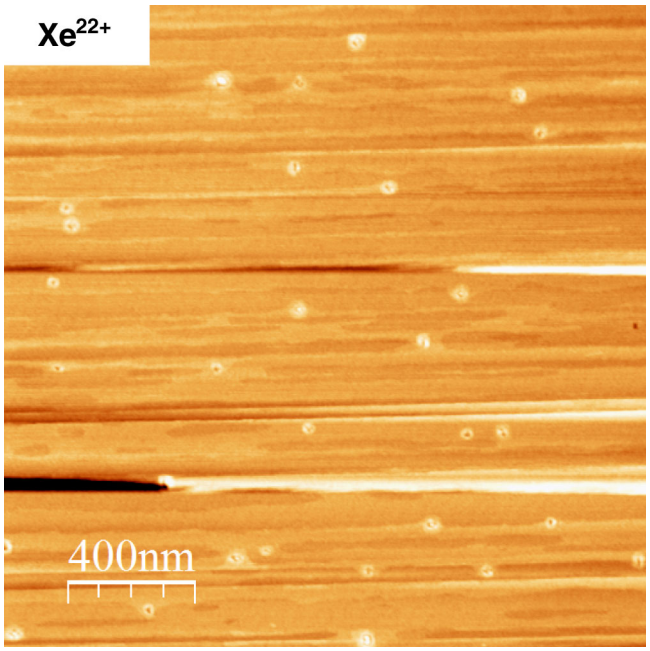

FIG. 1. SFM topographic images of LiF surfaces irradiated with 750 eV/amu Xe^{22+}.

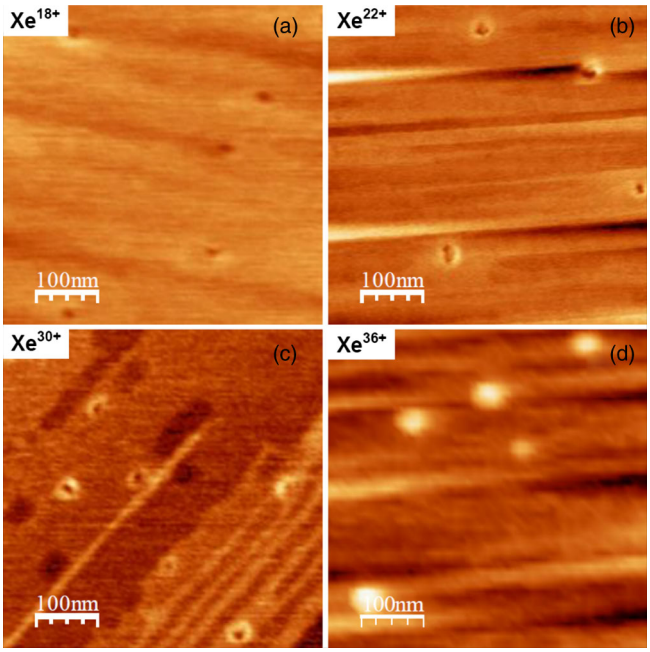

FIG. 2. (a) Pit, (b),(c) caldera, and (d) hillock surface nanostructures created by Xe^{Q+} ($Q = 18$, 22, 30, and 36) ions in LiF single crystals.

ions were extracted from the electron beam ion trap of the two-source facility at the Ion Beam Center of the Helmholtz-Zentrum Dresden-Rossendorf. After charge state separation by means of a 90° analyzing magnet, the ions were decelerated by a two-stage deceleration system to the desired kinetic energy of 100 keV (750 eV/amu). Utilizing an ion beam diameter of 1.5 mm, an area of 7×7 mm^2 was homogeneously irradiated by wobbling the sample holder. The ion fluence on the samples was in the range of 7×10^8 to 2×10^9 ions/cm^2. After irradiation, the surfaces were analyzed using a Nanoscope III (Bruker) scanning force microscope (SFM) operated in tapping mode under ambient conditions.

Depending on the charge state of the Xe^{Q+} ions and thereby on the potential energy three different types of nanostructures have been observed on the irradiated LiF surfaces. In all cases, the areal density of the features coincides well with the applied ion fluence as shown by way of example in Fig. 1 for caldera structures created by Xe^{22+} ions. Thus, every single ion impact results in the formation of a nanostructure. For the low charge states of $Q = 15$ and $Q = 18$ the structures are pits as shown in Fig. 2(a). Pit structures have already been observed on KBr and KCl surfaces after irradiations with charge states larger than 15 and 25, respectively [13,30]. On KBr the pits were only one monolayer deep. Here, the pits exhibit a mean depth of ~0.6 nm corresponding to about two atomic layers. The average lateral size of the pits increases from ~20 nm for $Q = 15$ to ~25 nm for $Q = 18$. The potential sputtering yield for such pits is around 11 000 and 18 000 atoms/ion, respectively. Upon increasing the charge state to $Q = 22$, the shape of the created structures changes. The pits are now surrounded by a rim protruding out of the surface as shown in Fig. 2(b). The rim height also depends on the potential energy and increases from 0.6 nm for $Q = 22$ to 1.4 nm for $Q = 30$. Similar caldera structures have been observed earlier on TiO_2 [16]. For the even higher charge states of $Q = 33$ and $Q = 36$ the shape of the structures changes now to hillocks with an average height of 1.0 and 1.5 nm, respectively. These kinds of structures have been investigated in detail on HCI irradiated CaF_2 surfaces [31].

A common feature for HCI induced nanostructures is the presence of a threshold in the potential energy that has to be exceeded in order to observe the created features [4]. It is obvious from the obtained results for LiF that two potential energy thresholds exist: one for the creation of the caldera-like structures and the other for hillocks. In the case of the calderas, the threshold is between 3.4 and 5.8 keV, whereas for the creation of the hillocks it is between 15.4 and 21.2 keV. In order to visualize the evolution of the nanostructures the rim height or pit depth was selected as a common parameter, which is studied as a function of the potential energy (see Fig. 4). Typical SFM images and line profiles used for the rim height or pit depth estimation for each shape of the created nanostructures are shown in Fig. 3. The rim height of the structures increases nonlinearly from 0 to 1.5 nm by increasing the potential energy from $E_p = 3.4$ keV to $E_p = 27.8$ keV. In contrast to the rim height, the depth decreases until it vanishes around the potential energy threshold for hillock creation.

Based on the observed change of both the shape and size of the created nanostructures as a function of potential

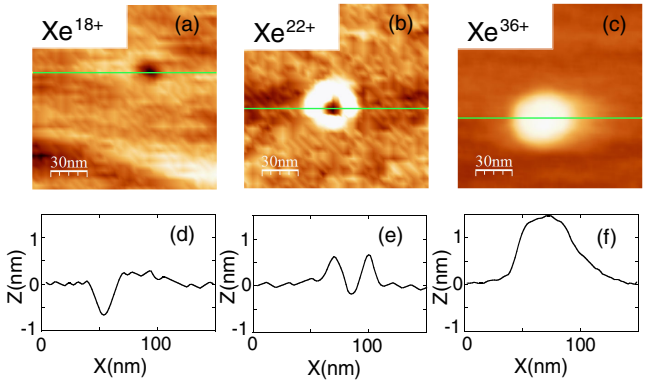

FIG. 3. SFM topographic image (top) and line profile (bottom) of one pit (a,d), caldera structure (b,e), and hillock (c,f) induced by Xe^{18+}, Xe^{22+}, and Xe^{36+}, respectively.

energy, a combination of nonthermal and thermal effects were suggested. The transition between these regimes is correlated with surpassing the critical potential energy needed for melting a crystalline LiF region. In order to describe and analyze the effect of the ion potential energy E_p in the creation of the observed nanostructures, we adopted the inelastic thermal spike model for insulators, originally used for swift heavy ions [32]. Within the modified model, the dissipation of potential energy is performed in two steps. First, the potential energy of the projectile is deposited on a femtosecond time scale into the electronic subsystem. In a second step, the energy is transferred to the lattice atoms on a picosecond scale, where they are heated up causing strong lattice deformations. The small volume, where the potential energy of the HCIs is deposited leads to a high energy density, which can be sufficient to induce a phase transformation in the impact region. For these low-velocity projectiles, the heat propagation can be considered in a hemispherical volume, assuming the crystal surface to be a reflecting boundary [33], when the heat conduction equation for the lattice reads

$$\rho C \frac{\partial T}{\partial t} = \frac{1}{r^2}\frac{\partial}{\partial r}\left(r^2 K \frac{\partial T}{\partial r}\right) + N, \tag{1}$$

where $T(r,t)$ is the temperature distribution to be found, $C(T)$ is the heat capacity, and $K(T)$ is the thermal conductivity. Instead of the supplementary equation for electronic diffusion and thermal conduction, used in the two-temperature thermal spike model, the heat transfer to the lattice $N(r,t)$ was employed in a simple analytical form [32]:

$$N(r,t) = \frac{2E_p}{(4\pi\sigma)^{3/2}\tau}\exp\left(-\frac{t}{\tau} - \frac{r^2}{4\sigma^2}\right). \tag{2}$$

Here, the factor of 2 reflects the hemisphere geometry and

$$\sigma^2 = D_e t + r_0^2,$$

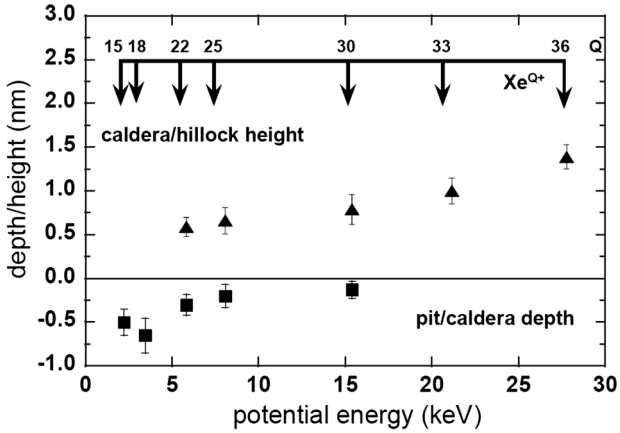

FIG. 4. Mean rim height (positive) and depth (negative) of nanostructures created in the LiF(100) surface by 750 eV/amu Xe^{Q+} as a function of potential energy. The ion charge states (Q) of the ions are shown in the upper horizontal scale.

where the electron diffusivity $D_e = 1.0\ \mathrm{cm}^2/\mathrm{s}$ and the electron-lattice relaxation time $\tau = 8 \times 10^{-14}$ s [34]. The initial radius of the free electron distribution is $r_0 = 1.0$ nm [32]. These parameters match the ones used in the thermal spike model for SHIs [32–34]. This is mainly based on the similarity between HCIs and SHIs in the energy deposition to the solid surface, which was demonstrated by observing similar structures in different materials [9,28]. Despite the fact that part of the ions' potential energy can be lost due to electron emission, we omit this effect as the retention part in the case of insulators is close to the total E_p [35].

The numerical solution of Eq. (1) is plotted in Fig. 5. When $T(r,t)$ reaches the melting temperature of LiF, $T_m = 1118$ K, the melting starts while keeping the temperature constant until the latent heat of fusion is absorbed. During the cooling down the solidification proceeds similarly at T_m, forming a plateau on $T(r,t)$, as shown in Fig. 5. The maximum outer radii of the partially (dashed line) and completely (solid line) molten region are used to calculate the enclosed hemispherical volume. The

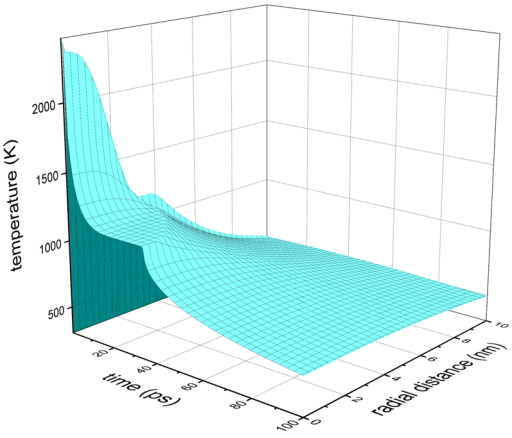

FIG. 5. Lattice temperature (T) as a function of time (t) and distance (r) from the ion impact site of HCIs of $E_p = 20$ keV.

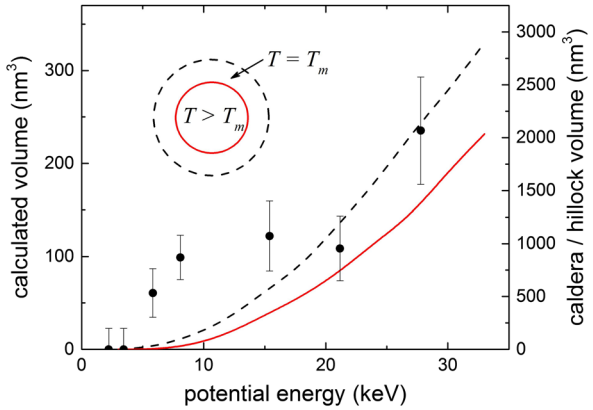

FIG. 6. The calculated volumes of the impact regions, where melting starts (dashed line) and is completed (solid line), and the caldera or hillock volume (black dots, right axis) as a function of ion potential energy.

completely molten volume ($T > T_m$) is smaller due to the latent heat, as shown in Fig. 6. The calculations showed that the melting occurs at a potential energy of about 6.0 keV, which is in fair agreement with the observed threshold of caldera formation. However, the volume of the protruded structures, which is estimated from the AFM profiles, appears to be larger than the calculated volumes. This fact is in agreement with previous results for CaF_2 [5,31], indicating that the induced melting triggers the appearance of the caldera or hillocks, but their size is rather determined by thermal expansion, which provides outward viscous flow and/or high-temperature plastic deformations, followed by rapid quenching.

The rim of the caldera structure results from the outward flow of the molten material followed by rapid quenching. In addition, the further increase of potential energy leads to a size increase of the molten zone until the crater of the caldera is closed. This transition is represented by a stepwise increase of the height of the caldera and hillock structures in the analyzed results, as shown in Fig. 3. Similarly, the volume of the created structures increases as a function of potential energy, as shown in Fig. 6.

The formation of pits for ions with potential energies below the threshold required for melting is not expected in view of the thermal spike model. However, for wide band gap materials with strong electron-phonon coupling the strong electronic excitations induced by the potential energy release, i.e., hot holes and electron-hole pairs, can cause lattice defect formation without melting by the creation of self-trapped holes and self-trapped excitons. Self-trapped excitons will decay in LiF into separated Frenkel pairs, namely H centers (F_2^- on an anion lattice site) and F centers (an electron localized in an F vacancy). H centers are stable in LiF at $T \leq 60$ K [36]. Above this temperature the H centers become mobile and can diffuse to the surface leading to the desorption of F^0. In addition, when F centers reach the surface, they can recombine with Li^+ leading to the desorption of Li^0. However, the creation and mobility of both F and H centers can be also affected by the presence of contained impurities. This model, originally developed for the electron and photon induced desorption of alkali halides [37], was used successfully to describe the formation of monatomic deep pits on KBr surfaces induced by highly charged Xe ions [13]. Furthermore, the existence of a threshold for potential sputtering as well as the charge state dependence of the potential sputtering by multiple charged ions gave conclusive evidence for a defect-mediated sputtering mechanisms in LiF [38,39]. Electron stimulated desorption and sputtering by singly charged ions lead to the emission of only a few atoms per incident electron or ion, which desorb predominantly from weakly bound positions at step edges. For high fluence irradiations with electrons and slow moderately charged ions similar nanostructures were observed [13,40,41]. However, these structures are the result of nucleation and the coarsening of vacancies and vacancy clusters. For slow highly charged ions the energy deposition in the surface during the neutralization and deexcitation processes is very large leading to a high excitation density and thus to a high density of H and F centers in a small area at the surface. Consequently, pit structures are created directly by single ion impacts. The pits in our experiments are caused by the desorption of around ten LiF molecules per 100 eV of potential energy. This value is about 1 order of magnitude higher than the value reported in Refs. [38,42] for desorption induced by multiply charged ions.

In conclusion, we have shown that even in the same material slow highly charged ions can be used to create different types of nanostructures. This was demonstrated by observing three types of nanostructures, i.e., pit, caldera, and hillock structures in the (100) surface of LiF after irradiation with slow highly charged Xe^{Q+} ions. The shape and size of the created nanostructures were controlled by tuning the potential energy of the incident ions: pits for charge $Q = 15$–18, calderas for $Q = 22$–30, and hillocks for $Q = 33$–36. The height of the nanostructures increases by varying the potential energy from 3.4 to 27.8 keV. Probing the lattice heating following HCI impact by numerical calculations using the modified inelastic thermal spike model shows that for rim formation the lattice temperature should exceed the melting point. The formation of pits was in turn explained by defect-mediated desorption due to the high defect density induced by the potential energy deposition in a small volume.

A. S. E. would like to acknowledge the support by King Fahd University of Petroleum and Minerals (Projects No. RG1326 and No. IN151017). Parts from this research were carried out at the Ion Beam Center (IBC) of the Helmholtz-Zentrum Dresden-Rossendorf, a member of the Helmholtz Association.

*elsaid@kfupm.edu.sa
a_s_elsaid@mans.edu.eg
On leave from Physics Department, Faculty of Science, Mansoura University, 35516 Mansoura, Egypt.
†aumayr@iap.tuwien.ac.at

[1] O. Ochedowski, O. Osmani, M. Schade, B. K. Bussmann, B. Ban-d'Etat, H. Lebius, and M. Schleberger, Nat. Commun. **5**, 3913 (2014).
[2] R. A. Wilhelm, E. Gruber, R. Ritter, R. Heller, S. Facsko, and F. Aumayr, Phys. Rev. Lett. **112**, 153201 (2014).
[3] F. Roeder, G. Hlawacek, S. Wintz, R. Huebner, L. Bischoff, H. Lichte, K. Potzger, J. Lindner, J. Fassbender, and R. Bali, Sci. Rep. **5**, 16786 (2015).
[4] F. Aumayr, S. Facsko, A. S. El-Said, C. Trautmann, and M. Schleberger, J. Phys. Condens. Matter **23**, 393001 (2011).
[5] A. S. El-Said, R. A. Wilhelm, R. Heller, S. Facsko, C. Lemell, G. Wachter, J. Burgdorfer, R. Ritter, and F. Aumayr, Phys. Rev. Lett. **109**, 117602 (2012).
[6] A. S. El-Said, R. Heller, F. Aumayr, and S. Facsko, Phys. Rev. B **82**, 033403 (2010).
[7] R. Ritter, G. Kowarik, W. Meissl, A. S. El-Said, L. Maunoury, H. Lebius, C. Dufour, M. Toulemonde, and F. Aumayr, Vaccum **84**, 1062 (2010).
[8] A. S. El-Said, Nucl. Instrum. Methods Phys. Res., Sect. B **282**, 63 (2012).
[9] A. S. El-Said, R. A. Wilhelm, R. Heller, S. Facsko, C. Trautmann, and F. Aumayr, Nucl. Instrum. Methods Phys. Res., Sect. B **269**, 1234 (2011).
[10] M. Terada, N. Nakamura, Y. Nakai, Y. Kanai, S. Ohtani, K.-i. Komaki, and Y. Yamazaki, Nucl. Instrum. Methods Phys. Res., Sect. B **235**, 452 (2005).
[11] M. Tona, H. Watanabe, S. Takahashi, N. Nakamura, N. Yoshiyasu, M. Sakurai, T. Terui, S. Mashiko, C. Yamada, and S. Ohtani, Surf. Sci. **601**, 723 (2007).
[12] R. Ritter, R. A. Wilhelm, R. Ginzel, G. Kowarik, R. Heller, A. S. El-Said, R. M. Papaleo, W. Rupp, J. R. C. Lopez-Urrutia, J. Ullrich, S. Facsko, and F. Aumayr, Europhys. Lett. **97**, 13001 (2012).
[13] R. Heller, S. Facsko, R. A. Wilhelm, and W. Moller, Phys. Rev. Lett. **101**, 096102 (2008).
[14] R. Ritter, R. A. Wilhelm, M. Stöger-Pollach, R. Heller, A. Mucklich, U. Werner, H. Vieker, A. Beyer, S. Facsko, A. Gölzhäuser, and F. Aumayr, Appl. Phys. Lett. **102**, 063112 (2013).
[15] V. Mussi, F. Somma, P. Moretti, J. Mugnier, B. Jacquier, R. M. Montereali, and E. Nichelatti, Appl. Phys. Lett. **82**, 3886 (2003).
[16] M. Tona, Y. Fujita, C. Yamada, and S. Ohtani, Phys. Rev. B **77**, 155427 (2008).
[17] R. M. Montereali, M. Piccinini, and E. Burattini, Appl. Phys. Lett. **78**, 4082 (2001).
[18] P. Bilski, Nucl. Instrum. Methods Phys. Res., Sect. B **251**, 121 (2006).
[19] W. S. Tsang, C. L. Mak, and K. H. Wong, Appl. Phys. A **77**, 693 (2003).
[20] K. Schwartz, C. Trautmann, and R. Neumann, Nucl. Instrum. Methods Phys. Res., Sect. B **209**, 73 (2003).
[21] C. Trautmann, M. Toulemonde, J. M. Costantini, J. J. Grob, and K. Schwartz, Phys. Rev. B **62**, 13 (2000).
[22] A. S. El-Said, M. Cranney, N. Ishikawa, A. Iwase, R. Neumann, K. Schwartz, M. Toulemonde, and C. Trautmann, Nucl. Instrum. Methods Phys. Res., Sect. B **218**, 492 (2004).
[23] M. Boccanfuso, A. Benyagoub, K. Schwartz, C. Trautmann, and M. Toulemonde, Nucl. Instrum. Methods Phys. Res., Sect. B **191**, 301 (2002).
[24] A. S. El-Said, Ph. D. thesis, Heidelberg University, 2004.
[25] A. S. El-Said, R. Neumann, K. Schwartz, and C. Trautmann, Nucl. Instrum. Methods Phys. Res., Sect. B **245**, 250 (2006).
[26] K. Schwartz, C. Trautmann, A. S. El-Said, R. Neumann, M. Toulemonde, and W. Knolle, Phys. Rev. B **70**, 184104 (2004).
[27] A. S. El-Said, R. Neumann, K. Schwartz, and C. Trautmann, Surf. Coat. Technol. **158–159**, 522 (2002).
[28] C. Müller, M. Cranney, A. El-Said, N. Ishikawa, A. Iwase, M. Lang, and R. Neumann, Nucl. Instrum. Methods Phys. Res., Sect. B **191**, 246 (2002).
[29] N. Khalfaoui, C. C. Rotaru, S. Bouffard, M. Toulemonde, J. P. Stoquert, F. Haas, C. Trautmann, J. Jensen, and A. Dunlop, Nucl. Instrum. Methods Phys. Res., Sect. B **240**, 819 (2005).
[30] R. A. Wilhelm, Ph. D. thesis, TU Dresden (2014).
[31] A. S. El-Said, R. Heller, W. Meissl, R. Ritter, S. Facsko, C. Lemell, B. Solleder, I. C. Gebeshuber, G. Betz, M. Toulemonde, W. Moller, J. Burgdorfer, and F. Aumayr, Phys. Rev. Lett. **100**, 237601 (2008).
[32] M. Toulemonde, C. Dufour, A. Meftah, and E. Paumier, Nucl. Instrum. Methods Phys. Res., Sect. B **166–167**, 903 (2000).
[33] M. Karlušić and M. Jakšić, Nucl. Instrum. Methods Phys. Res., Sect. B **280**, 103 (2012).
[34] A. Meftah, F. Brisard, J. M. Costantini, E. Dooryhee, M. Hage-Ali, M. Hervieu, J. P. Stoquert, F. Studer, and M. Toulemonde, Phys. Rev. B **49**, 12457 (1994).
[35] D. Kost, S. Facsko, W. Moller, R. Hellhammer, and N. Stolterfoht, Phys. Rev. Lett. **98**, 225503 (2007).
[36] K. T. Noriaki Itoh, Radiat. Eff. **98**, 269 (1986).
[37] M. Szymonski, J. Kołodziej, Z. Postawa, P. Czuba, and P. Piatkowski, Prog. Surf. Sci. **48**, 83 (1995).
[38] T. Neidhart, F. Pichler, F. Aumayr, H. P. Winter, M. Schmid, and P. Varga, Phys. Rev. Lett. **74**, 5280 (1995).
[39] F. Aumayr and H. Winter, Philos. Trans. R. Soc., A **362**, 77 (2004).
[40] R. Bennewitz, S. Schär, V. Barwich, O. Pfeiffer, E. Meyer, F. Krok, B. Such, J. Kolodzej, and M. Szymonski, Surf. Sci. **474**, L197 (2001).
[41] F. Krok, S. R. Saeed, Z. Postawa, and M. Szymonski, Phys. Rev. B **79**, 235432 (2009).
[42] G. Hayderer, S. Cernusca, M. Schmid, P. Varga, H. P. Winter, F. Aumayr, D. Niemann, V. Hoffmann, N. Stolterfoht, C. Lemell, L. Wirtz, and J. Burgdorfer, Phys. Rev. Lett. **86**, 3530 (2001).